Suppression of spin bath dynamics for improved coherence of multi-spin-qubit systems
Supplementary Information

Supplementary Figures

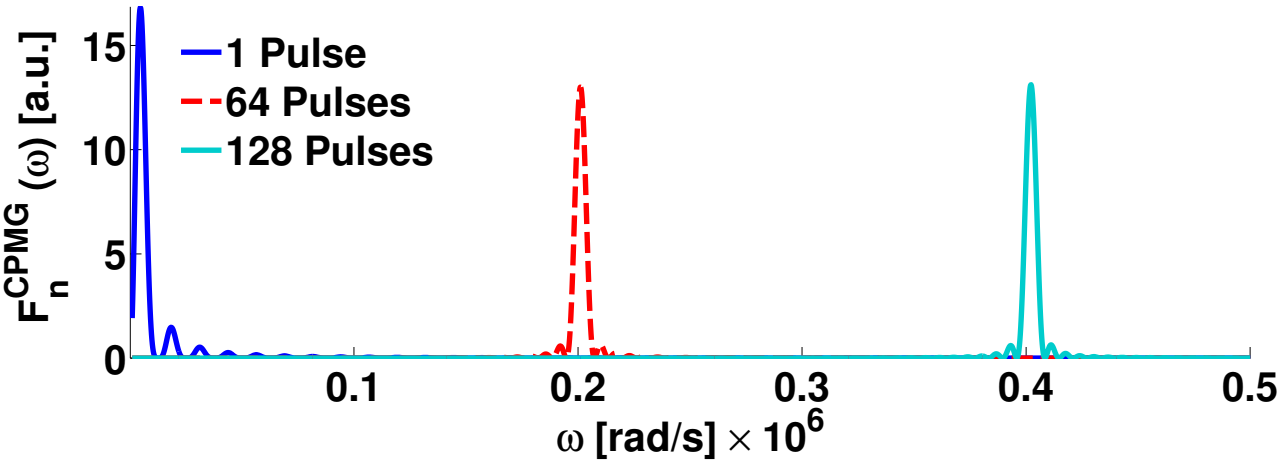

Supplementary Figure S1. CPMG filter functions. Calculated filter function $F_n^{\mathrm{CPMG}}(\omega)$ for three examples of the number n of CPMG pulses ($n = 1, 64, 128$).

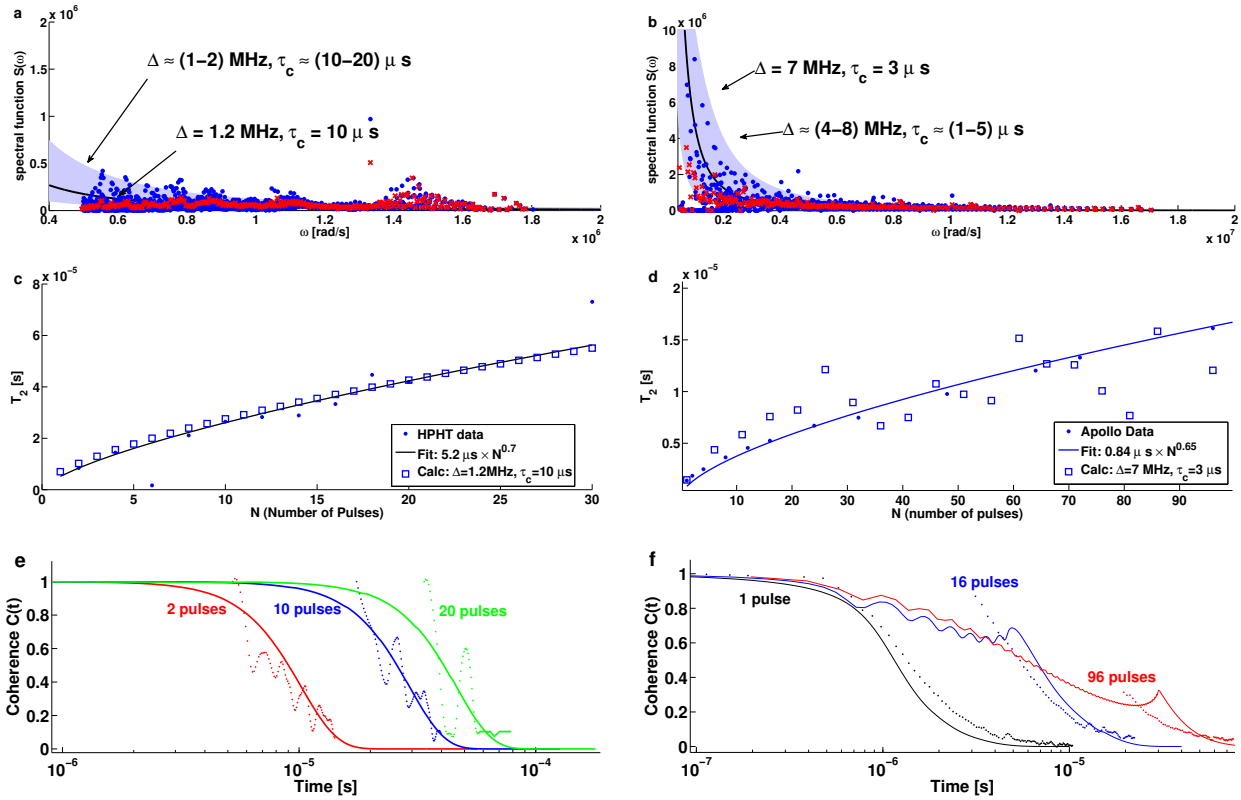

Supplementary Figure S2. Spectral analysis of the HPHT (left) and Apollo (right) samples. (a),(b) Derived values for the spin bath spectral functions $S_n(\omega)$ for all CPMG pulse sequences (blue dots) and average values at each frequency (red crosses). Each blue dot represents a pulse sequence with a specific duration t and number of pulses n, such that the probed frequency is $\omega = \pi n/t$. Also shown is the best fit Lorentzian for the mean spectral function $\langle S_n(\omega)\rangle_n$ (solid black line), and a range of best-fit Lorentzians for the individual spectral functions $S_n(\omega)$ for each CPMG pulse sequence (light-blue band). (c),(d) Scaling of T_2 with the number n of CPMG pulses: derived from NV spin coherence decay data $C_n(t)$ (dots); fit of data to a power law (solid line); and synthesized from the average-fit Lorentzian spin bath spectrum (open squares), which yields a consistent fit. (e),(f) Examples of measured NV multi-spin coherence as a function of time $C_n(t)$ for CPMG pulse sequences with different numbers of pulses n (solid lines), and the corresponding synthesized curves calculated using the average-fit Lorentzian spin bath spectrum (dots).

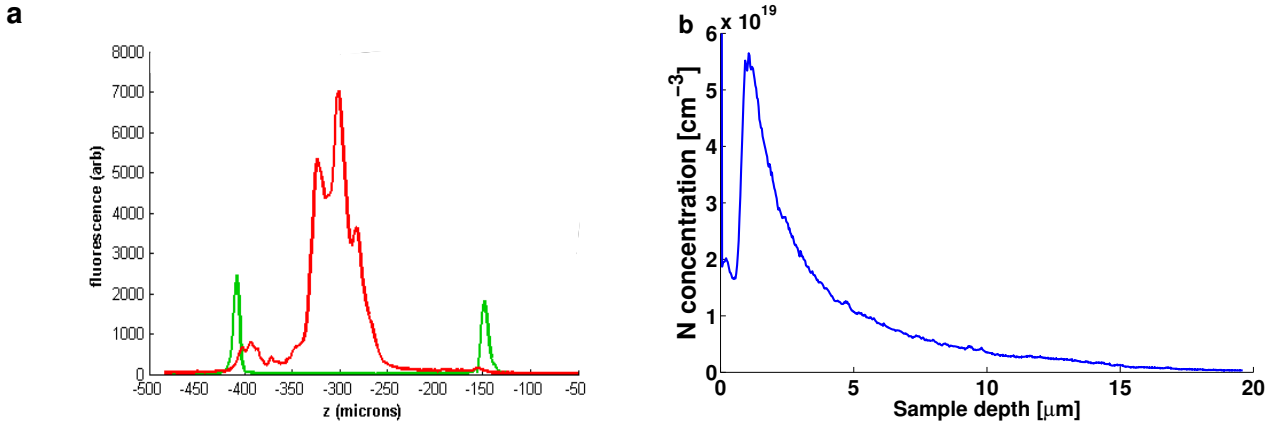

Supplementary Figure S3. Measurements of inhomogeneities in the ^{12}C and Apollo samples. (a) Confocal scan of NV fluorescence and hence concentration (red) as a function of depth in the ^{12}C sample. The green line indicates the surfaces of the sample as measured by enhanced reflection of the green excitation light. (b) Inhomogeneity of N concentration in the Apollo sample as measured using secondary ion mass spectroscopy (SIMS).

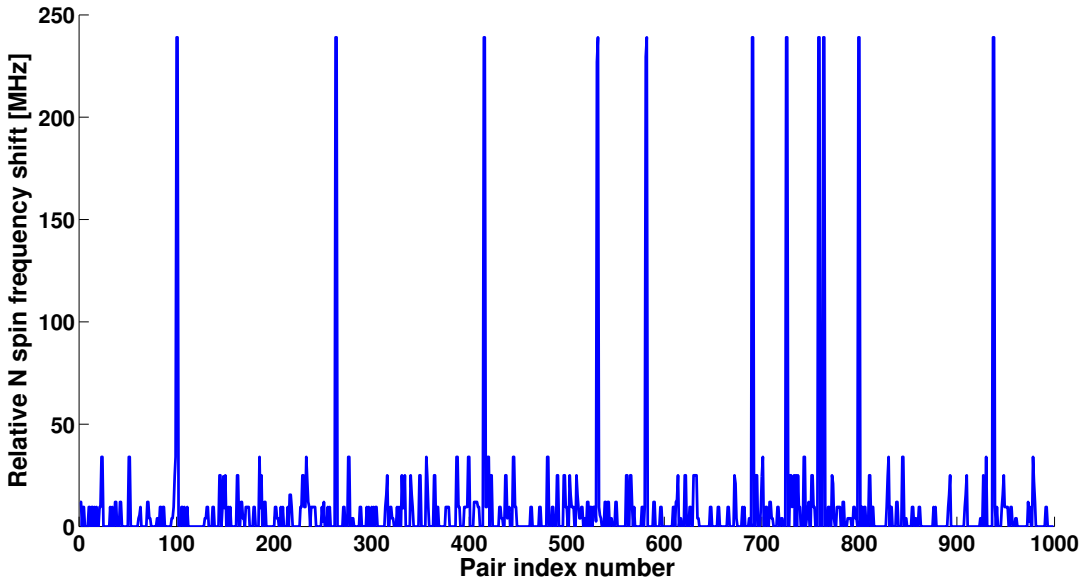

Supplementary Figure S4. Monte Carlo simulation of the ^{13}C-induced Overhauser effect. Example results of Monte Carlo simulation of relative frequency shift between 1000 pairs of N electronic spins induced by hyperfine interactions with ^{13}C nuclear spin impurities that are randomly distributed in a diamond lattice at the natural abundance concentration of 1.1%.

Supplementary Methods

Details of spectral analysis For each CPMG pulse sequence (and hence value of n) applied to each sample, we extract the decoherence functional $\chi_n(t) = -lnC_n(t)$ (see Eq. (1) in the main text) from the relevant NV multi-spin coherence data $C_n(t)$, such as that shown for the ^{12}C sample in Fig. 2a in the main text. The measured coherence $C_n(t)$ is well fit by a stretched exponential $e^{-(t/T_2)^p}$, where the value of p varies between 1 and 3 related to dynamics of the spin environment and ensemble inhomogeneous broadening (see section below on multi-spin averaging). This behavior is consistent with a Lorentzian spin bath spectrum and indicates that N spin impurities are the dominant source of NV spin decoherence. The effects of ^{13}C nuclear spin impurities are discussed in the main text. The second most important electronic spin impurities are NVH defects, which are an order of magnitude less abundant than N impurities [1]. The contribution of instantaneous spin diffusion due to interactions between neighboring NV spins and MW-induced spin flips [2] is also negligible, as the NV Rabi frequency for typical MW power ($\sim$ 10 MHz) is large compared to the NV electronic spin transition linewidth ($\sim$ 3 MHz), and the NV dipolar coupling timescale (proportional to the inverse of the dipolar coupling energy) is at least an order of magnitude longer than the longest measured NV spin coherence time.

Using the measured $C_n(t)$ data we derive values for the spin bath spectral function $S_n(\omega)$ for each CPMG pulse sequence by deconvolving $\chi_n(\omega)$ with the filter function $F_n^{\mathrm{CPMG}}(\omega t)$ (Supplementary Figure S1). The resulting values for the spectral functions $S_n(\omega)$ for all CPMG pulse sequences (i.e., all values of n) are plotted together in Fig. 2b in the main text. Note that the average data (red crosses) in Fig. 2b in the main text are calculated by binning the full data set for $S_n(\omega)$ into 100 frequency values between 0 and 1 MHz. As a result of this binning procedure, a few data points exhibited abnormally small coherence at low frequency, perhaps due to technical noise, which at $\sim$ 150 kHz contributes two outliers to the averaged data.

We use two methods of analysis to characterize the underlying spin bath spectrum $S(\omega)$ in terms of the coupling strength Δ of the bath spins to the probed NV spins and the correlation time τ_c of the bath spins with each other (Supplementary Figure S2): in the first we separately fit each spectral function $S_n(\omega)$ to a Lorentzian, which provides individual-fit values for Δ and τ_c for each of the CPMG pulse sequences; and in the second we average all the $S_n(\omega)$ values for each ω and then fit the resulting mean spectral function $\langle S_n(\omega))\rangle_n$ to a Lorentzian, which provides single, average-fit values for Δ and τ_c.

The oscillations in the HPHT coherence decay data are a result of a nearby spin impurity (most likely a ^{13}C nuclear spin). The relevant data for the reconstruction of the N-bath spectral function is the envelope of the decay, which was minimally affected by the oscillations.

The coherence decay data for the Apollo sample exhibited some non-monotonic behavior, which was a result of the large coupling strength between NV spins and the spin-bath in this sample, producing semi-coherent interaction effects. These effects were beyond the weak coupling approximation assumed for the spectral decomposition procedure and indicate that higher-order corrections might be non-negligible in this case. However, it can be seen that the second-order theory we employed here for spectral analysis still reproduces the main features of the decoherence curves, as well as the scaling of the NV T_2 with the number of CPMG pulses n.

We note that the frequencies at which the data was taken are dictated by the pulse sequence durations and numbers of pulses and are therefore not always commensurate between different pulse sequences.

We also note that the frequency range of the HPHT data is small compared to the other samples due to: first the short NV spin coherence time, which limits measurement of the very low frequency response; and second the reduced signal-to-noise (as this was a single NV measurement using a confocal apparatus), which limits the measurement of pulse sequences with a large number of pulses, thus excluding very high frequency data.

Multi-spin averaging For measurements with the ^{12}C and Apollo samples, the coherence decay function ($C(t) = e^{-(t/T_2)^p}$) and the scaling of T_2 with the number of CPMG pulses were not fully consistent over all measurement timescales and pulse numbers. This inconsistency was largely a result of averaging over many NV spins in the field of view, which modifies the effective bath spectrum from a simple Lorentzian due to inhomogeneities in the local NV environment and the spin bath. To account for such effects, we used the best average-fit Lorentzian and then calculated the expected coherence decay $C_n(t)$ and scaling of T_2 with CPMG pulse number by averaging over 20 model realizations of the spin-bath spectra, with parameters normally distributed around the values extracted from the average-fit Lorentzian, and the FWHM of this distribution set at 50% of the central extracted values.

The ^{12}C sample (Element 6) is a high quality, pure sample, with a low concentration of N impurities ($\sim$ 1 ppm) and a very low concentration of other defects. The sample does not show N-induced steps frequently associated with CVD diamond, due to the low concentration of N in the growth process [3]. The N concentration was calibrated

by Element 6 during growth and then verified to be $\sim$ 1 ppm by bulk EPR measurements. Measurement of N inhomogeneity using SIMS was not possible due to the relatively high N-detection threshold of this method ($>$ 1 ppm). We performed confocal scans of the sample to measure the spatial distribution of NV centers (Supplementary Figure 3(a)), which showed less than a factor of two variation in NV concentration throughout the sample. With the reasonable assumption that N and NV concentrations are proportional to each other, we conclude that the N concentration in this sample is similarly homogeneous to within about a factor of two.

The Apollo sample contains a high concentration of N impurities ($\sim$ 100 ppm), which are the dominant source of decoherence for the NV spins. To characterize inhomogeneity of the N concentration, we performed SIMS measurements on this sample (see Supplementary Figure 3(b)). Again assuming the N and NV concentrations are locally proportional to each other, we determined the mean N concentration probed by NV fluorescence measurements, $\overline{n_{\rm N}}$, from a weighted average over the local N concentration $n_{\rm N}(z)$:

$$\overline{n_{\rm N}} = \frac{\int_0^Z dz n_{\rm N}^2(z)}{\int_0^Z dz n_{\rm N}(z)}. \tag{S1}$$

Using the SIMS data we find $\overline{n_{\rm N}} \simeq 2.6(1.7) \times 10^{19}[cm^{-3}] \simeq 150(100)$ ppm, which is consistent with the coupling strength Δ for this sample extracted using the spectral decomposition technique, with the uncertainties in this value, and with Monte Carlo simulations we performed of the spin environment (see below). In addition, our measurements were carried out on a confined lateral region of $\sim 10 \times 10$ μm^2 to suppress the effects of inhomogeneities on a larger scale. The SIMS measurements also indicate that within the detection limits (1 ppm) there are no other extrinsic defects present, such as Boron or Si.

The HPHT sample also contains a high concentration of N impurities ($\sim$ 50 ppm). The low NV density of this sample allowed us to make single NV measurements using a confocal apparatus. Therefore, possible inhomogeneities of the N concentration do not affect the measured data. We measured NV centers in the central region of the HPHT sample, in the 100 growth sector, which was characterized by SIMS to have an N concentration of approximately $50 - 150$ ppm, consistent with our spectral decomposition value for the coupling strength Δ.

In summary, for all three samples the values we find for Δ using spectral decomposition are consistent with independent measurements and estimates of the N concentration, which therefore suggests that sample inhomogeneities are within expected ranges and understood to within a factor of 2-3. As a result, we have confidence that the values provided by spectral decomposition for the N spin-bath correlation time $\tau_{\rm c}$ in the HPHT and Apollo samples are an order of magnitude longer than the expected values given by a simple model of the N spin-bath that ignores N-^{13}C interactions, for the estimated values of N concentration for these two samples.

We note that a long spin-bath correlation time was also measured in an HPHT sample in [4] using a different method than the spectral decomposition technique presented here, further supporting our results. We also note that the results we obtained via spectral decomposition could not be recreated with any combination of Δ and $\tau_{\rm c}$ that follow the expected scaling with N concentration, regardless of the actual value of the assumed concentration and including inhomogeneous effects. Therefore, the combined results from the three samples, along with the independent measurements and estimates of N concentration and inhomogeneity, and the consistency of the extracted values for Δ, strongly support the validity of the unexpectedly long correlation time $\tau_{\rm c}$ observed in the HPHT and Apollo samples.

Lorentzian parameters for an N dominated bath For the samples measured in this work, N electronic spins (P1 centers) are the dominant environment coupling to NV spins. Thus, the expected parameters of the Lorentzian bath spectra can be derived from electronic dipolar interactions. The dipolar interaction energy between electronic spins is given by $U_{\rm dip} \approx \alpha n_{\rm N}$, where $\alpha \approx 3.3 \times 10^{-13}$ s^{-1}cm^3 and $n_{\rm N}$ is the N concentration [5]. Therefore the parameters of the Lorentzian spectrum are estimated to be $\Delta \approx U_{\rm dip}$ and $\tau_{\rm c} \approx 1/U_{\rm dip}$.

^{13}C induced broadening of N spin resonance Inhomogeneous broadening of an ensemble of N electron spin resonances in diamond due to proximal ^{13}C nuclear spin impurities is dominated by the strong N-^{13}C contact hyperfine interaction (compared to the weaker dipolar contribution, see [6, 7]). Therefore, the inhomogeneous broadening energy ΔE does not scale simply with the concentration of ^{13}C. To make a realistic estimate of ΔE, we carried out a Monte-Carlo simulation of 1000 pairs of N spin impurities, each with a different random distribution of ^{13}C spin impurities in a diamond lattice at their natural abundance of 1.1%. The calculated relative electronic spin resonance frequency shift for each N pair is plotted in Supplementary Figure S4. We find the average value of this detuning $\approx$ 9.5 MHz and the standard deviation $\approx$ 30 MHz, with a few rare events in which a ^{13}C occupies the nearest lattice to the N, producing a frequency shift $\sim$ 300 MHz. We conclude from this simulation that $\Delta E \sim$ 10 MHz, which is consistent with the suppression of N spin bath dynamics revealed by the spectral decomposition measurements and analysis.

Classes of P1 centers in diamond The electronic wavefunction of the P1 center (N impurity in the present case) is anisotropic and can be directed along each of the nearest C bonds. Therefore, there are generally 4 different classes of P1 centers. With a static magnetic field aligned along one of the axes, the hyperfine interaction separates the P1 center's electronic spin resonance into 5 different energies, depending on the class of P1 center (aligned with magnetic field or not) and the N nuclear spin state. This splitting is expected to suppress electronic spin flip-flops between P1 centers with different resonance energies. However, since this effect should be equally manifest in all samples regardless of the concentration of ^{13}C impurities, and since it can maximally account for a factor of 5 change, we conclude that it is not the dominant mechanism underlying the observed order-of-magnitude increase in the correlation time of the electronic spin bath in the presence of finite nuclear spin impurity concentration, as described in the main text.

[1] Edmonds, A. M. *et al.* Production of oriented nitrogen-vacancy color centers in synthetic diamond. *ArXiv e-prints* (2011). 1112.5757.

[2] Salikhov, K., Dzuba, S. & Raitsimring, A. The theory of electron spin-echo signal decay resulting from dipole-dipole interactions between paramagnetic centers in solids. *Journal of Magnetic Resonance (1969)* **42**, 255 – 276 (1981).

[3] Martineau, P. M. *et al.* Identification of Synthetic Diamond Grown Using Chemical Vapor Deposition (CVD). *Gems & Gemology* **40**, 2–25 (2004).

[4] de Lange, G. *et al.* Controlling the quantum dynamics of a mesoscopic spin bath in diamond. *Arxiv:* 1104.4648v1 (2011).

[5] Taylor, J. M. *et al.* High-sensitivity diamond magnetometer with nanoscale resolution. *Nat. Phys.* **4**, 810–816 (2008).

[6] Cox, A., Newton, M. E. & Baker, J. M. ^{13}C, ^{14}N and ^{15}N endor measurements on the single substitutional nitrogen centre (p1) in diamond. *Journal of Physics: Condensed Matter* **6**, 551 (1994).

[7] Barklie, R. C. & Guven, J. ^{13}C hyperfine structure and relaxation times of the p1 center in diamond. *J. Phys. C* **14**, 3621 (1981).